

A Theoretical Study of Gas-Phase Unimolecular Decomposition of Simulants of the Nerve Agent VX

Xiao Shan,^{*,†} Mark R. Sambrook,[‡] and David C. Clary[†]

[†]*Physical and Theoretical Chemistry Laboratory, Department of Chemistry, University of
Oxford, South Parks Road, Oxford, OX1 3QZ, United Kingdom*

[‡]*CBR Division, Dstl Porton Down, Salisbury, SP4 0JQ, United Kingdom*

E-mail: xiao.shan@chem.ox.ac.uk

Abstract

In order to further understand and support approaches for the degradation and destruction of toxic chemicals, the thermal decomposition of the nerve agent VX through possible pericyclic hydrogen transfer reactions is investigated using simulant molecules. A total of four simulant molecules are studied. Three of them have only one possible H transfer site while the other has two. They are chosen to bring physical insights into individual steps of the pericyclic reaction mechanism as well as the possible existence of competing mechanisms. The unimolecular reaction rate constants at high pressure limit are calculated. Geometries of stationary structures on the potential energy surfaces are calculated with the MP2 method as well as the B3LYP and M06-2X functionals and 6-311++G(d,p), jul-cc-pVTZ, aug-cc-pVTZ basis sets. The barrier heights are corrected using energy values obtained at CBS/QB3 level of theory. The contribution of the quantum tunneling effect to the reaction rate constants is included using one-dimensional semiclassical transition state theory. Adiabatic barrier heights, reaction rate constants, and the branching ratio of the competing mechanisms are reported.

1. Introduction

The organophosphorus (OP) Chemical Warfare Agents (CWAs), such as sarin (GB), soman (GD), VX, and the toxic organophosphorus pesticide amiton (VG) are highly toxic nerve agents that inhibit the acetylcholine esterase enzyme.^{1,2} Varied research efforts into understanding and mitigating against the effects of such materials include, amongst others, studies into surface-sorption,³⁻⁶ formulation-based decontamination,⁷⁻⁹ novel catalysts¹⁰⁻¹⁴ and destruction via thermal degradation,^{15,16} or incineration. Recently, experimental and theoretical studies^{15,16} showed that it is possible to have a complete thermal decomposition of GB at temperatures of 350 – 500 °C (ca. 623 – 773 K) after a short period of time (0.062 – 0.5 s). During this thermal decomposition, GB undergoes a pericyclic hydrogen-transfer reaction via a 6-membered ring structured transition state (TS). A schematic of this mechanism is shown in Fig. 1. In another study, Ash *et al.*¹⁵ analysed all possible thermal decomposition mechanisms for GB and GD at temperatures between 300 – 1000 K and found that the reaction through this 6-membered ring TS is the dominating pathway for both molecules. Other mechanisms with 5-membered ring TS or smaller rings have considerable larger barriers, typically over 30 kcal/mol (~ 126 kJ/mol) higher.¹⁵ In order for an OP molecule to undergo this pericyclic H-transfer it must satisfy two conditions. Firstly it must contain an ester of phosphonate acid to have the adequate π -electron configuration. Secondly the alcoholic side chain of the ester must be longer than a methyl group with at least one H atom attached to the secondary C atom so that the TS of the pericyclic reaction has the most stable 6-membered ring structure. In the case of VX, shown in Fig. 2, two pericyclic reaction pathways are possible. The phosphorus containing product of each reaction pathway can then undergo pericyclic reaction again to give the final thermal decomposition products.

Due to the toxicity of CWAs and regulation under the Chemical Weapons Convention (CWC), experimental studies with actual CWAs can be challenging to accomplish. *Ab initio* calculations, on the other hand, do not have the safety issues, but can face computational

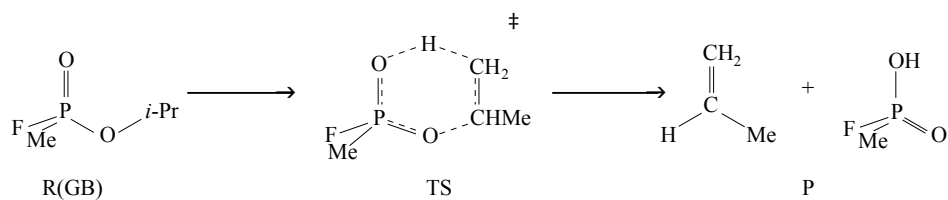


Figure 1: Schematic of the mechanism of the pericyclic H-transfer reaction of GB. The abbreviations "Me" and "*i*-Pr" indicate the methyl and isopropyl groups, respectively.

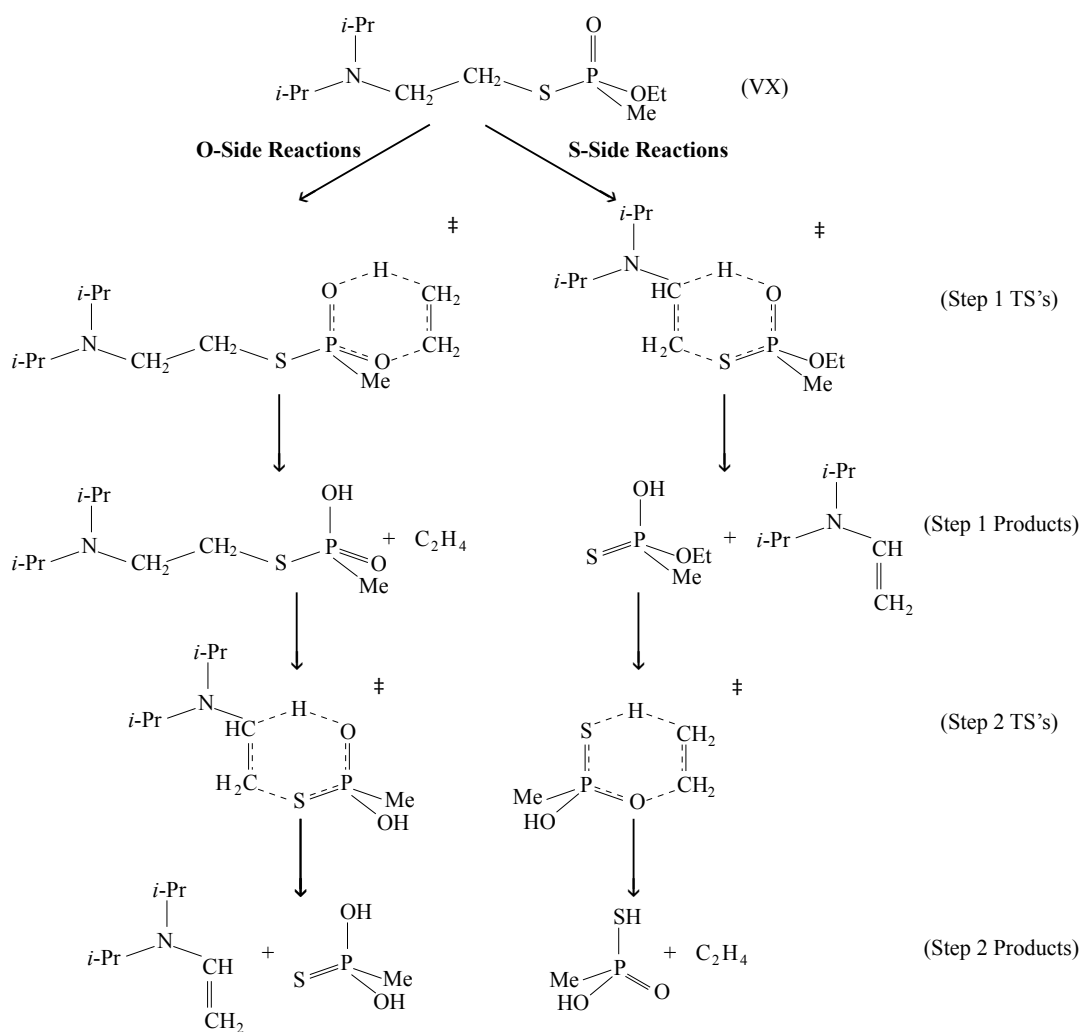


Figure 2: Schematics of proposed mechanisms of the pericyclic H-transfer reactions of VX. The abbreviations "Me", "Et", and "*i*-Pr" indicate the methyl, ethyl, and isopropyl groups, respectively.

challenges due to the size of the molecules. Performing dynamic studies on OP CWAs, such as computing unimolecular decomposition reaction rate constants, is by no means a simple task. As a result, simulant molecules are often used in research instead. One good example is dimethyl methylphosphonate (DMMP).^{17–24} A great number of experimental and theoretical works have been dedicated on the decomposition of DMMP alone.^{20–22} In 2009, Yang *et al.*²⁰ investigated the gas-phase unimolecular decomposition of DMMP. The calculated barrier height for the lowest barrier is 73.1 kcal/mol (~ 306.1 kJ/mol) indicating that this decomposition is unlikely to occur in gas-phase. However, the structure of DMMP does not fit condition 2 mentioned in the first paragraph. The alcoholic side chain of DMMP has only a methyl group and thus it cannot form a 6-membered ring TS for a pericyclic reaction. The barrier height of DMMP is very similar to the values found for GB and GD in Ash *et al.*¹⁵ with 5- or 4-membered ring TS's.

In the current study, to investigate the proposed mechanisms of VX thermal decomposition shown in Fig. 2, we analyse two groups of different simulant molecules, shown in Fig. 3(a) and (b). The first group of molecules in Fig. 3(a) consists of only one possible pericyclic H-transfer site, they are therefore potential simulants for each individual steps of the proposed mechanism shown in Fig. 2. Note that the step 1 TS of the S-side reactions and step 2 TS of the O-side reactions share the same simulant molecule (A2 shown in Fig. 3(a)). The simulant molecules A1 and A3 correspond to step 1 TS of O-side reactions and step 2 TS of S-side reactions, respectively. *O,S*-Diethyl methylphosphonothiolate, shown in Fig. 3(b), is in the second group and we shall refer to it as simulant B in the remainder of the paper for convenience. It has the same core atomic combination around the P atom as VX. In addition, it has two possible pericyclic H-transfer sites, the same as VX. It should be noted that all of the simulant molecules have a chiral centre at the P atom. However, since the alcoholic side chains are only ethyl groups, none of the TS's of the simulant molecules would introduce an additional chiral centre, which was found in the case for GB¹⁶ and would also for VX. For all of the simulant molecules, the *R*- or *S*-enantiomers would have the same

kinetic and thermodynamic properties. In the current study, we therefore perform our calculations on only the *R*-enantiomers of these molecules, as shown in Fig. 3. In the remainder of the paper, the notation "*R*-" is omitted for convenience.

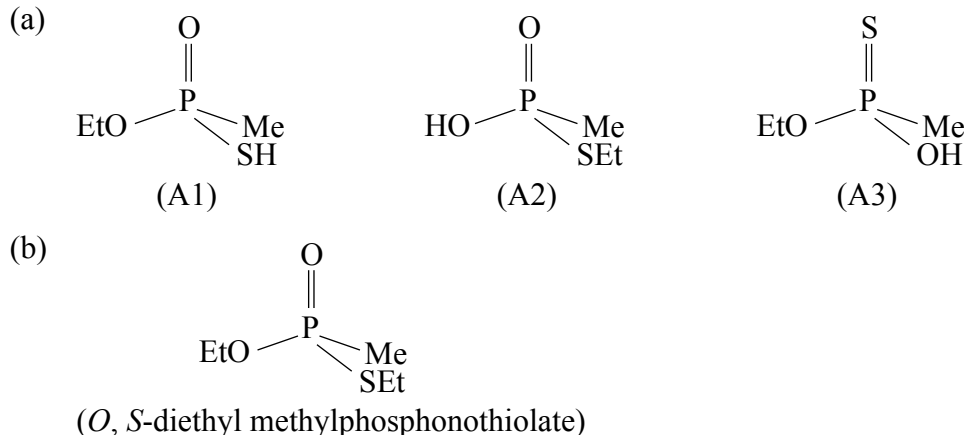


Figure 3: Schematics of the simulant molecules (a) with one pericyclic H-transfer site and (b) with two pericyclic H-transfer site. The abbreviations "Me" and "Et" indicate the methyl and ethyl groups, respectively.

As an H atom is directly involved in all of these pericyclic reactions, quantum tunneling effect will play an important role in the reaction mechanism especially at low temperatures. In a recent study of GB thermal decomposition,¹⁶ it has been found that even at relatively high temperature (600 – 700 K) quantum tunneling makes a considerable contribution to the rate constant. In the current study, we employ the one-dimensional semiclassical transition state theory (1D SCTST) to include the tunneling effect. The SCTST has been applied to the study of reaction rate constants of numerous bimolecular^{25–40} and unimolecular^{16,41} reactions. The 1D SCTST is a simplification of SCTST in a reduced dimensionality framework such that only the reaction mode vibration (1D) in the TS is treated anharmonically. This method significantly reduces the amount of *ab initio* calculation required³⁶ and yet maintains the level of accuracy of a full-dimensional analysis. In the previous studies,^{16,36,40,42} the combination of geometry optimization and vibrational analyses using the second-order Møller-Plesset perturbation theory (MP2) method and single point energy correction to the barrier height at coupled cluster level including single, double and perturbative triple excita-

tions (CCSD(T)) level has been proven to provide accurate rate constants when comparing to either experimental or high level quantum scattering results. However, for molecules as large as *O,S*-diethyl methylphosphonothiolate, even in the 1D case the above combination of theories can be computationally expensive to perform. We, therefore, tested several density functional theories (DFT) with a combination of different basis sets to find a computationally cheap and yet reasonably accurate level of calculation that can in the future grant access to the studies of chemical nerve agents such as VX and VG.

The remainder of the article is organised in the following way. A brief outline of the theoretical tools used in this study are outlined in Section 2. Section 3 presents details of the computational methods used. The results of geometry optimizations, vibrational analyses, testing of the DFT methods and rate constants calculations are shown and discussed in Section 4. The key findings of this study are in Section 5.

2. Theoretical Background

2.1. 1D SCTST

In the current study, we focus on the calculation of the canonical reaction rate constants, $k(T)$, of the unimolecular pericyclic H-transfer reactions. At high pressure limit, the standard TST rate constant is given by

$$k_{\text{TST}}(T) = \frac{1}{h} \frac{Q_{\text{rot}}^{\ddagger} Q_{\text{vib}}^{\ddagger}}{Q_{\text{rot}}^{\text{R}} Q_{\text{vib}}^{\text{R}}} k_{\text{B}} T \exp(-\Delta V_f k_{\text{B}}^{-1} T^{-1}), \quad (1)$$

where Q^{\ddagger} and Q^{R} are the partition functions of the TS and the reactant and ΔV_f is the forward reaction adiabatic barrier height. Note that in unimolecular reactions, only the rotational and vibrational partition functions are included in this equation. Although being the cheapest method in terms of computational cost to calculate the reaction rate constant, the TST neglects important effects such as barrier recrossing and quantum tunneling. The

quantum tunneling of H atom is of particular importance in H-transfer reactions. To correct this, various methods have been developed over the past few decades. We employ the one-dimensional semiclassical transition state theory (1D SCTST)^{16,35,36,40,42}. In this method, the rate constant is given by

$$k_{1\text{D SCTST}}(T) = \frac{1}{h} \frac{Q_{\text{rot}}^{\ddagger} Q_{\text{vib}}^{\ddagger}}{Q_{\text{rot}}^{\text{R}} Q_{\text{vib}}^{\text{R}}} \int_{E_{\text{thresh}}}^{\infty} P(E_v) \exp(-E_v k_{\text{B}}^{-1} T^{-1}) dE_v. \quad (2)$$

Note that in a unimolecular reaction, some of the vibrational modes of the TS and the reactant may have very similar frequencies and the vibrational partition functions for those modes in Eqs. 1 and 2 are likely to cancel out.¹⁶ The vibrational frequencies of the lowest energy conformer of the reactants and TS's for the reactions studied here are reported in the Supporting Documents. Comparing these two equations, we can see that the partition function part of a standard TST and a 1D SCTST are exactly the same. The tunneling contribution is included in the 1D SCTST via the cumulative reaction probability, $P(E_v)$, given by

$$P(E_v) = \{1 + \exp[2\theta(E_v)]\}^{-1}, \quad (3)$$

where

$$\theta(E_v) = \frac{\pi}{2x_{\text{FF}}} \{-\Omega + [\Omega^2 + 4x_{\text{FF}}(\Delta V_f + G_0 - E_v)]^{1/2}\}, \quad (4)$$

with

$$\Omega = \text{Im}(\hbar\omega_{\text{F}}), \quad (5)$$

$$G_0 = \frac{\hbar^2}{64} \left(\frac{f_{\text{FFFF}}}{\omega_{\text{F}}^2} - \frac{5}{9} \frac{f_{\text{FFF}}^2}{\omega_{\text{F}}^4} \right), \quad (6)$$

and

$$x_{\text{FF}} = \frac{\hbar^2}{16\omega_{\text{F}}^2} \left(f_{\text{FFFF}} - \frac{5f_{\text{FFF}}^2}{3\omega_{\text{F}}^2} \right) \quad (7)$$

where ω_{F} is the reaction mode vibrational frequency. f_{FFF} and f_{FFFF} are respectively the third and fourth order derivatives of the potential energy surface (PES) with respect to

the reaction mode vibration. In practice, the only computation required in a 1D SCTST in addition to a standard TST is the computation of f_{FFF} and f_{FFFF} . This can be easily achieved via numerical differentiation of single point energies at a minimum of 4 displacement geometry points. One can also apply the Richardson extrapolation^{43–45} to improve the accuracy of the numerical differentiations. The details of applying this method to SCTST calculation have been reported previously^{16,36}. Recent studies showed that a Richardson extrapolation to the order of 2, that is a set of energies of 8 displacement geometries, is sufficient for the accuracy of the derivatives^{16,36}. It should be noted that although the additional cost of a 1D SCTST to a standard TST is 8 single point calculations, the 1D SCTST rate constant is very sensitive to the value of ω_F because of its significant involvement in Eqs. 4 to 7. However, it is possible for calculations performed at different levels of theory to give similar standard TST rate constants but completely different 1D SCTST ones. We shall discuss this in more detail in Section 4.1.

The theories discussed so far are related to the original SCTST developed by Miller and co-workers.^{25–28,46} In this form of SCTST, the calculation of the barrier penetration integral in Eq. 4 is equivalent to the WKB integral for a symmetric Eckart potential.^{47,48} The reactant asymptote of such a potential is not the quantum mechanical threshold energy, E_{thresh} .

$$E_{\text{thresh}} = \max(\Delta V_f - \Delta V_r, 0). \quad (8)$$

where ΔV_r is the reverse adiabatic barrier of a reaction. To correct this, a piece-wise continuous asymmetric Eckart barrier model was proposed by Wagner.⁴⁷ It is often referred to as the deep-tunneling (DT) correction to the SCTST.^{16,35,36,39,40,42} The calculation of $\theta(E_v)$ with the DT corrected barrier can be found in Wagner *et al.*⁴⁷ This DT corrected form of SCTST is employed in the current study. In order to construct this new barrier, ΔV_r is required. Therefore the total cost of 1D SCTST in addition to a standard TST is 8 single point energy calculations and the reverse adiabatic barrier height.

2.2. Hindered Rotor

Similar to the sarin molecule in our previous study¹⁶, all of the simulant molecules and TS's consist of several low frequency hindered rotor vibrations. We employ the multi-structural method based on including all structures/conformers generated by internal rotation, or the so-called MS-AS method to correct the errors introduced when these modes are treated as harmonic oscillators in the partition functions. The MS-AS is an approximate yet powerful treatment to multi-dimensional hindered rotor vibrations developed by Truhlar and co-workers^{49–52}. Detailed discussion of this method can be found in Ref. 52, only a brief outline is given here.

The corrected TST rate constant is written as Eq. 1 with the partition functions replaced by the conformational-rovibrational partition functions,

$$k_{\text{TST,HR}}(T) = \frac{1}{h} \frac{Q_{\text{con-rotvib}}^{\text{MS-AS, TS}}}{Q_{\text{con-rotvib}}^{\text{MS-AS, R}}} k_{\text{B}} T \exp(-\Delta V_f k_{\text{B}}^{-1} T^{-1}). \quad (9)$$

where

$$Q_{\text{con-rovib}}^{\text{MS-AS}} = \sum_{j=1}^J [Q_{\text{rot},j} Q_j^{\text{HO}} c_{\text{HR}} \exp(-U_j k_{\text{B}}^{-1} T^{-1})]. \quad (10)$$

Essentially, the total rovibrational partition function of a molecule is calculated as an energy weighted sum of rovibrational partition functions of the torsional conformers of the molecule. Here $Q_{\text{rot},j}$ and Q_j^{HO} are the rotational and harmonic oscillator vibrational partition function of the j -th conformer respectively. The term $c_{\text{HR},j}$ then corrects the vibrational partition function of the hindered rotor vibrational modes. It is given by

$$c_{\text{HR},j} = Z_j \prod_{\tau=1}^t f_{j,\tau}, \quad (11)$$

For each individual structure of the J -total conformer, we have

$$f_{\tau} = \frac{\bar{\omega}_{\tau} \sqrt{2\pi\beta k_{\tau}}}{M_{\tau}} \exp\left(-\frac{I_{\tau}}{M_{\tau}^2 k_{\text{B}} T}\right) I_0\left(\frac{I_{\tau}}{M_{\tau}^2 k_{\text{B}} T}\right), \quad (12)$$

and

$$Z = g + (1 - g) \frac{\prod_{m=1}^{F-t} \bar{\omega}_m^{-1} \prod_{\tau=1}^t \bar{\omega}_\tau^{-1}}{\prod_{m=1}^F \omega_m^{-1}} \left(\frac{|\det \mathbf{D}|}{\prod_{\tau=1}^t I_\tau} \right)^{1/2}, \quad (13)$$

where

$$g = \left[\prod_{\tau=1}^t \tanh \left(\frac{\sqrt{2\pi k_\tau k_B^{-1} T^{-1}}}{M_\tau} \right) \right]^{1/t}. \quad (14)$$

and $\bar{\omega}_\tau$, k_τ , M_τ and I_τ are respectively the frequency, force constant, number of minima and moment of inertia for the τ -th hindered rotor. I_0 is a modified Bessel function, ω_m is the harmonic frequency of the m -th vibration, and $\bar{\omega}_m$ is the frequency of the m -th non-hindered-rotor vibrational modes.⁵² \mathbf{D} is the kinetic energy matrix for internal rotation^{53–55}.

If one assumes that these hindered rotor modes are not coupled to the reaction mode, a treatment similar to that of the TST rate constant can be applied to the 1D SCTST⁴⁰. The 1D SCTST rate constant is simply

$$k_{1D \text{ SCTST}}(T) = \frac{1}{h} \frac{Q_{\text{con-rotvib}}^{\text{MS-AS, TS}}}{Q_{\text{con-rotvib}}^{\text{MS-AS, R}}} \int_{E_{\text{thresh}}}^{\infty} P(E_v) \exp(-E_v k_B^{-1} T^{-1}) dE_v. \quad (15)$$

Note that this correction of hindered rotor vibrational modes does not affect the 1D SCTST calculation discussed in Section 2.1. For a full-dimensional (FD) SCTST calculation, however, one needs to take the coupling between the normal vibrational modes and hindered rotor modes into consideration. Detailed discussion on this topic is beyond the scope of the current study. Studies of FD SCTST on a reaction system that consists of one hindered rotor can be found in Ref. 39.

3. Computational Method

Gaussian09 software⁵⁶ was used for the quantum chemistry calculations in this study. In our previous studies on various systems,^{16,36,40,42} the optimized geometries and vibrational frequencies of the stationary points on the PES were usually obtained at the MP2 level of

theory. The barrier heights were then corrected at the CCSD(T) level. Since the molecules include P and S atoms, diffuse functions are required in the basis set. This then makes the calculation very expensive computationally. It is then desirable to find an alternative method that is less costly but is able to maintain the level of accuracy. In the current study, we use simulant A1 as a testing case. The benchmark has geometries and frequencies at the MP2/jul-cc-pVTZ⁵⁷ level and energies at the CSB/QB3^{58,59} level. We test the density functional theories (DFT) B3LYP and M06-2X⁶⁰ in combination of basis sets including aug-cc-pVTZ^{61,62}, jul-cc-pVTZ⁵⁷ and 6-311++G(d,p)^{63,64} for the geometry optimization and vibrational analyses. The barrier corrections were all done at the CBS/QB3 level. The 1D SCTST calculation of the third and fourth order derivatives of the PES as well as the hindered rotor analyses were performed at the same level of theory as the geometry optimizations. For the other simulant molecules, we used the most accurate DFT and CBS/QB3 in the calculation.

4. Results and Discussions

4.1. Simulant A1

We present in Fig. 4(a) and (b) respectively the optimized geometries of the conformers of the reactant and TS of simulant A1 calculated at the MP2/jul-cc-pVTZ level of theory. One interesting feature of this molecule is the rotation of the SH group about the S–P single bond. In the reactant, there are only 2 possible conformations, one approximately pointing in the same direction as the P=O double bond while the other pointing in the opposite direction. This is because the P atom is bonded to one of the O atoms through a π bond and the 3p-electrons in the S atom are also delocalised into this π system, and hence the O=P–S–H retains an almost planar geometry. Note that this feature no longer exists in the TS (Fig. 4(b)), because both of the P–O bonds have a double bond feature, and the 3p-electrons in the S are no longer delocalised into this system. This results in the TS having

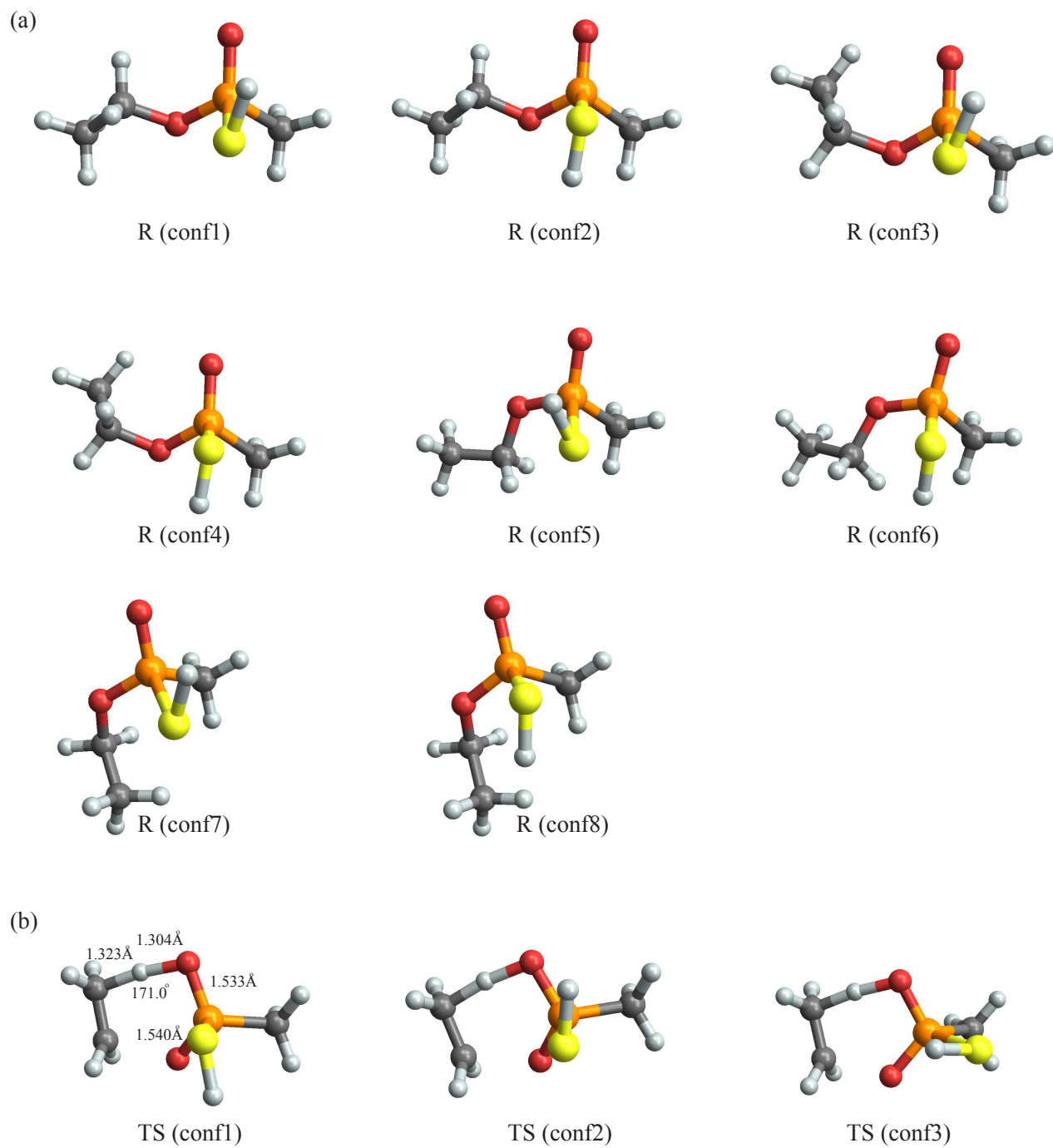


Figure 4: The optimized geometries of the conformers of (a) the reactant and (b) TS for pericyclic H transfer reaction of simulant A1.

3 conformers due to the rotation of the SH group about the S–P bond.

The values of the key bond lengths and angles of conformer 1 for the TS calculated using different levels of theories are shown in Table 1. Note that the values of MP2 results are also marked on Fig. 4(b) to provide a clear indication of the chemical bonds listed here. The results of all the methods are in very close agreement to each other. The two M06-2X calculations show better agreement than the three B3LYP calculations to the MP2 results on the bond distances related to the transferring H atom, the O–H and H–C lengths. For the bond angle between these two bonds, the B3LYP results are very similar to each other and are approximately 1° higher than the MP2 result. The M06-2X methods only slightly underestimate this bond angle by 0.44% and 1.18% for the aug-cc-pVTZ and 6-311++G(d,p) basis sets respectively. From the geometry optimization point of view, all of the DFT results are very close to the ones obtained at the MP2 level.

Table 1: Table of optimized key bond lengths and angles for TS conformer 1 of simulant A1. Bond lengths are in Å and bond angles are in degrees. The terms "jvtz" and "avtz" indicate the jul-cc-pVTZ and aug-cc-pVTZ basis sets, respectively.

Method	B3LYP			M06-2X		MP2
Basis sets	jvtz	avtz	6-311++G(d,p)	avtz	6-311++G(d,p)	jvtz
O–P	1.5356	1.5355	1.5403	1.5289	1.5319	1.5397
P=O	1.5268	1.5268	1.5319	1.5199	1.5239	1.5326
O–H	1.3575	1.3574	1.3607	1.2946	1.2934	1.3042
H–C	1.2894	1.2893	1.2889	1.3359	1.3380	1.3225
O–H–C	172.15	172.17	171.25	170.29	169.02	171.04

The calculated values of the adiabatic barrier heights are reported in Table 2. Here we take the values calculated at MP2/jul-cc-pVTZ//CBS/QB3 level of theory as the benchmark. It can be seen that all the calculated barrier heights once corrected with the CBS/QB3 single point energies have very good agreement to the corresponding benchmark values. The B3LYP method clearly underestimates the forward barrier height. However, the B3LYP/aug-cc-pVTZ and B3LYP/6-311++G(d,p) reverse barrier heights are quite accurate with the B3LYP/aug-cc-pVTZ value being the closest to the benchmark out of all the none CBS-

corrected values. The M06-2X functional has a much better performance than the B3LYP in general. The M06-2X/aug-cc-pVTZ having the least combined error for the barrier heights in both directions. Interestingly the CBS corrected barriers for the M06-2X geometries underestimates both the forward and reverse barrier when compared to the benchmark.

Table 2: Table of reaction energetics of the pericyclic H transfer reaction for simulant A1. All values are in the unit of kJ/mol. The term "(CBS)" denotes the single point energies were calculated using the CBS/QB3 method with the geometries optimized at the corresponding level of theory. The benchmark values are in bold.

Method	Basis sets	ΔV_f	ΔV_r	ΔV_f (CBS)	ΔV_r (CBS)
B3LYP	jul-cc-pVTZ	147.37	103.67	187.01	118.07
	aug-cc-pVTZ	166.44	119.85	187.05	118.10
	6-311++G(d,p)	168.46	116.33	186.67	118.16
M06-2X	aug-cc-pVTZ	187.63	117.43	186.43	117.82
	6-311++G(d,p)	191.13	114.17	185.72	117.60
MP2	jul-cc-pVTZ	188.12	115.52	187.40	119.69

In Table 3, we compare the calculated reaction mode vibrational frequencies, which are of great importance to a 1D SCTST rate constant calculation as explained in Section 2.1. It shows that for the same DFT method, the difference between the values of the frequency calculated using different basis sets are almost negligible. However, when comparing to the MP2 results, the M06-2X results have a much closer agreement than the B3LYP ones. In fact, the B3LYP method underestimates the frequency of the reaction mode by over 20%. This affects the 1D SCTST tunneling correction through the shape of the barrier in the SCTST calculation, shown in Fig. 5. It is very clear that all the B3LYP barriers are much wider than the MP2 ones, and hence it will result in smaller tunneling probability and in turn underestimation of the rate constant. On the other hand, the M06-2X barriers, including the M06-2X/aug-cc-pVTZ without CBS correction barrier, have very good agreement to the MP2 one.

We now discuss the hindered rotor calculations. The calculated reactant and TS conformer energies relative to their corresponding conformer 1 shown in Fig. 4 are in Table

Table 3: Table of reaction mode vibrational frequencies for simulant A1. All values are in the unit of cm^{-1} .

Method	Basis sets	ω_F
B3LYP	jul-cc-pVTZ	1131.72I
	aug-cc-pVTZ	1130.61I
	6-311++G(d,p)	1125.95I
M06-2X	aug-cc-pVTZ	1383.61I
	6-311++G(d,p)	1382.32I
MP2	jul-cc-pVTZ	1441.64I

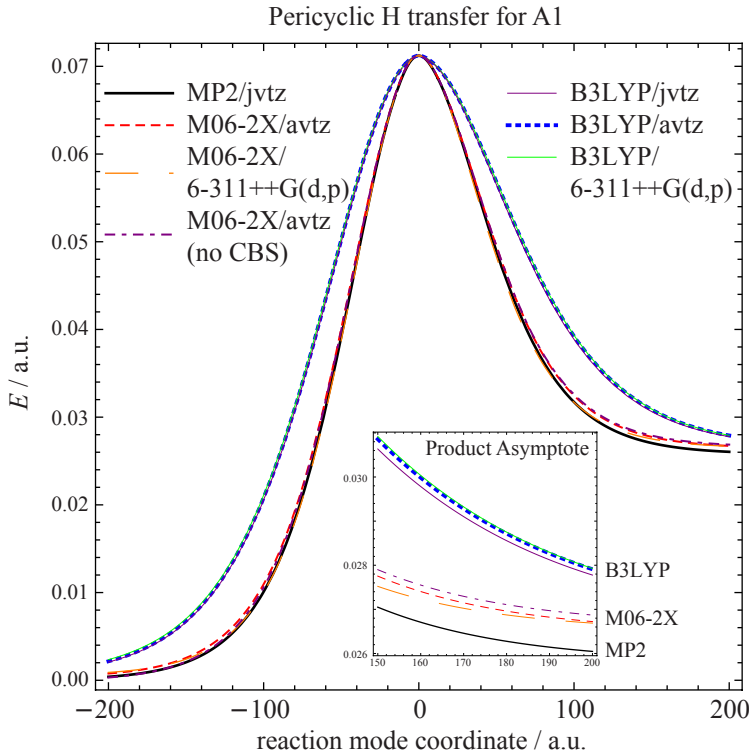


Figure 5: The one-dimensional potential for the pericyclic H-transfer reaction of A1 constructed using informations in Tables 2 and 3. The product region of the constructed potentials is shown in the inset.

Table 4: Table of conformer relative energies of reactant and TS’s for the pericyclic H transfer reaction of simulant A1. All values are in the unit of kJ/mol.

		M06-2X/aug-cc-pVTZ	M06-2X/6-311++G(d,p)	MP2/jul-cc-pVTZ
R	conf 1	0.00	0.00	0.00
	conf 2	2.03	2.86	2.46
	conf 3	-0.128	-0.0624	0.507
	conf 4	1.71	2.64	2.78
	conf 5	15.0	17.3	15.8
	conf 6	20.8	24.7	24.7
	conf 7	21.3	24.1	22.6
	conf 8	28.4	32.3	31.9
TS	conf 1	0.00	0.00	0.00
	conf 2	0.14	-0.24	0.34
	conf 3	2.83	3.34	3.73

4. Note that since the hindered rotor treatment does not affect the tunneling correction (discussed in Section 2.2) and the B3LYP calculations fails to construct a sufficiently accurate barrier (shown in Fig. 5), only the MP2 and M06-2X results are presented. It can be seen that the results from all three computational methods have relatively good agreement. Largest energy differences between M06-2X and MP2 results are found in conformers 6 to 8, which are over 20 kJ/mol higher in energy than the most stable conformer. Their contributions to the total rovibrational partition function are almost negligible, the differences in their energies therefore would have a very small effect on the overall rate constant. The reactant conformers, on the other hand, can be divided into two groups. Conformer 1, 2, 3, and 4 in Fig. 4 are close in energy, while the other conformers corresponding to rotating the ethyl group across the O–P bond have much higher energies. All three TS conformers have very similar energies. Note that the conformer 3 of the reactant at M06-2X/aug-cc-pVTZ and M06-2X/6311++G(d,p) levels and conformer 2 of the TS at M06-2X/6311++G(d,p) are lower in energy than that of their corresponding conformer 1. However, our CBS calculations show that the conformer 1 for the reactant and TS calculated at all level of theories has lowest adiabatic energy. Therefore, the reaction energetics and reaction mode frequencies reported in Tables 2 and 3 were calculated using geometries of conformer 1.

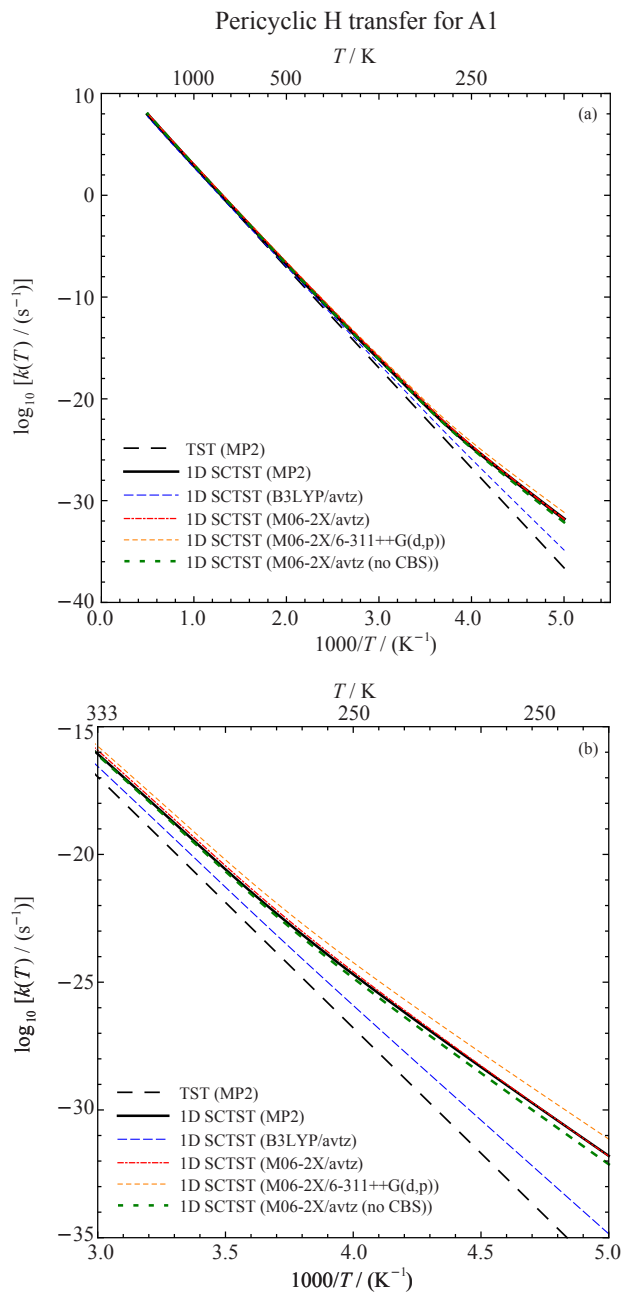


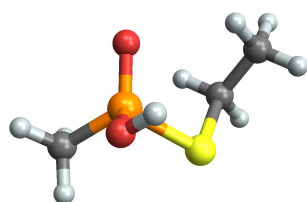
Figure 6: Reaction rate constants of the pericyclic H transfer for A1 in the temperature range of (a) 200 K to 2000 K and (b) 200 K to 300 K. The term "avtz" indicates the aug-cc-pVTZ basis set. All except one the calculations used their corresponding CBS/QB3 energies reported in Table 2. The dotted dark green curve on both plot shows the rate constant calculated using purely the M06-2X/aug-cc-pVTZ results.

Fig. 6(a) shows the calculated reaction rate constants for temperature ranging from 200 K to 2000 K. The numerical values of the rate constants can be found in the supporting documents. It can be seen that all the rate constants converge at high temperature as expected, since the forward reaction barriers calculated at different level of theory are very similar as shown in Table 4. All of the 1D SCTST results suggest that quantum tunneling has an important contribution at temperatures typically below 400 K. For instance, at 200 K the MP2 1D SCTST rate constant (solid black curve) is over 6×10^4 times higher than the TST one (dashed black curve). It is also very clear that due to the wider constructed 1D barrier discussed earlier, the B3LYP method fails to capture this tunneling contribution. At 200 K, the B3LYP rate constant (dashed blue curve) is over 1000 times slower than the MP2 one. On the other hand, all the M06-2X results (the dash-dotted red curve, the dashed orange curve and the dotted green curve) show very good agreement to the MP2 result. To further investigate the accuracy of these results, we show in Fig. 6(b) the calculated rate constants between 200K to 300K. The M06-2X/6-311++G(d,p) method consistently overestimates the rate constant when comparing to the MP2, while the M06-2X/aug-cc-pVTZ results with or without CBS/QB3 energy correction have excellent agreement to the MP2 results. We shall therefore in the following sections use the M06-2X/aug-cc-pVTZ method in combination of CBS/QB3 for correcting the barrier heights to calculate the reaction rate constants for the pericyclic H transfer reactions for the other simulant molecules. We will also show the results without CBS/QB3 calculation to further analyse the accuracy of this DFT method on barrier height calculations.

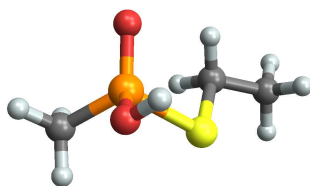
4.2. Simulant A2 and A3

The conformer geometries of the reactant and TS for the H-transfer reaction of A2 are shown in Fig. 7(a) and (b) respectively. One obvious geometrical difference between the conformers of A2 and A1 is that the hindered rotation of OH in A2 produces only one conformer while the SH rotation in A1 had two reactant conformers and three TS conformers. In Fig. 8, we

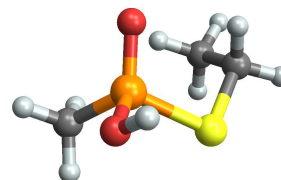
(a)



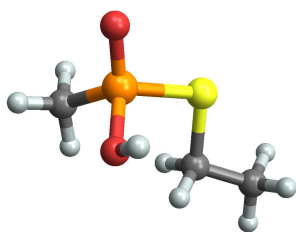
R (conf1)



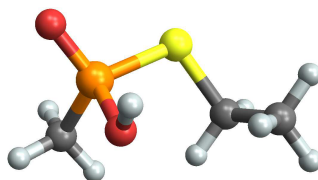
R (conf2)



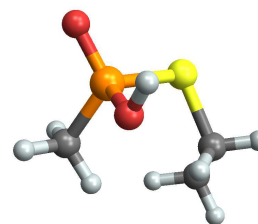
R (conf3)



R (conf4)

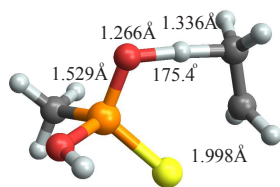


R (conf5)



R (conf6)

(b)



TS (conf1)

Figure 7: The optimized geometries of the conformers of (a) the reactant and (b) TS for pericyclic H transfer of simulant A2.

show the one dimensional potential energy curve of this OH rotation in A2 conformer 1 of the reactant (as the solid black curve) and the TS (as the solid red curve), taking the geometries shown on Fig. 7 being the starting geometry of rotation angle of 0° . These potential energy curves for A2 have only one peak at approximately 180° and 220° for the reactant and TS respectively, and they both have a "shoulder" type shape at around 50° to 100° respectively. Note that we performed mode redundant geometry optimization for this region with small angular step sizes, and found no local minima. This single minima behaviour is found for all the reactant conformers shown in Fig. 7(a). This particular behaviour is due to the interaction between the delocalised π -electrons in the O=P–S group and the H atom in the OH group. The OH group plays a crucial role here, and it is therefore important to note that this one-minima hindered rotor is not a general case for larger molecules, such as simulant B, VX, or VG, where the O atom is attached to an ethyl or longer groups.

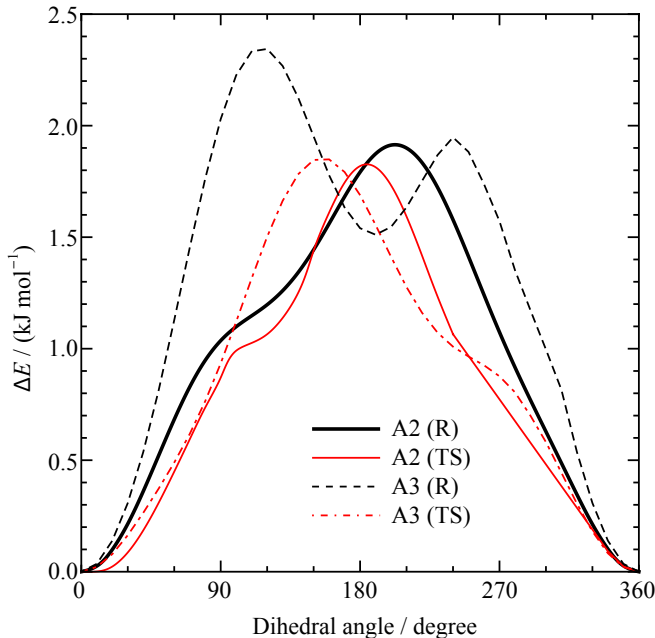


Figure 8: One dimensional potential energy curve of of the OH rotation in conformer 1 of the reactants and in the TS for A2 and A3 reactions.

In Fig. 9(a) and (b) we present the geometries of the reactant and TS conformers for the A3 reaction. The conformers of the A3 reactant shows similar behaviour to that of A1 having

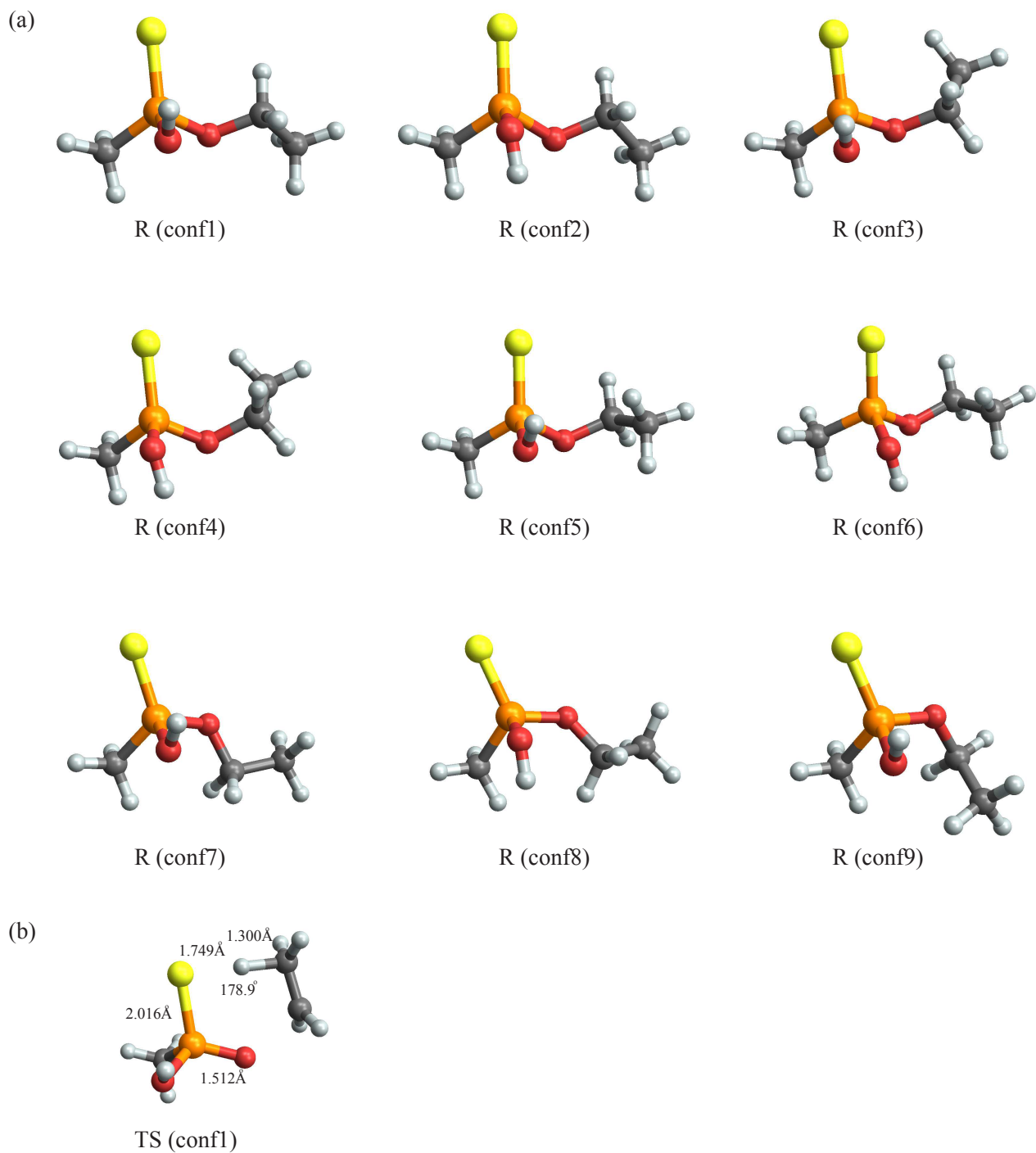


Figure 9: The optimized geometries of the conformers of (a) the reactant and (b) TS for pericyclic H transfer of the simulant A3.

two minima across the OH hindered rotation. Since the S and P atoms have low energy d-orbitals that are involved in the bonding, both O–P=S groups can have delocalisation of π -orbitals. It is important that the system consists of both S and P atoms. If the P atom is replaced by a C atom, this double delocalisation would not be observed. This results in the H atom on the OH group being in the same plane as the O–P=S group. In contrast, the TS for A3 reaction has only one conformer similar to the TS of A2. This is again due to the interaction between the H atom and the delocalised π -electrons. Note that in the TS, since the S atom is bonding towards the transferring H atom, it is no longer involved in the bonding between the OH group and P atom, and hence breaks the delocalisation found in A3 reactants. The one-dimensional potential energy curves of the OH hindered rotation in the conformer 1 of the A3 reactant and the A3 TS are shown in Fig. 8.

Table 5: Table of conformer relative energies of reactant for the pericyclic H transfer reaction of simulants A2 and A3. All values are in the unit of kJ/mol.

A2		A3			
conf 1	0.00	conf 1	0.00	conf 7	12.7
conf 2	2.75	conf 2	12.9	conf 8	37.2
conf 3	2.30	conf 3	0.193	conf 9	18.0
conf 4	7.19	conf 4	15.3		
conf 5	8.22	conf 5	1.55		
conf 6	7.28	conf 6	15.9		

The energies of the A2 and A3 conformers are listed in Table 5. The A2 conformers have energy differences within 10 kJ/mol, which is much smaller than that of the A3 conformers. Together with the energies of A1 conformers listed in Table 4 and the conformer geometries shown in Figs. 4, 7 and 9, we can see that rotation about P–S bonds has smaller effects on the energy than the rotation about P–O bonds. In addition, the rotation involving the ethyl group is energetically easier than the rotation of OH or SH groups. In the case of A2, since all the conformer geometries are results of ethyl group rotation, the conformers are close in energy.

In Table 6, we show the pericyclic H transfer reaction energetics for A2 and A3. The

Table 6: Table of reaction energetics of the pericyclic H transfer reaction for simulants A2 and A3 with geometries, vibrational frequencies, and energies calculated at M06-2X/aug-cc-pVTZ level. "CBS" indicates a single point energy correction at CBS/QB3 level is applied. All values are in the unit of kJ/mol.

	ΔV_f	ΔV_f (CBS)	ΔV_r	ΔV_r (CBS)
A2	185.42	175.67	105.92	104.50
A3	197.36	184.05	97.42	100.36

values were computed in such a way that the geometries and zero point energies were calculated at the M06-2X/aug-cc-pVTZ level, single point energy calculations were then done using CBS/QB3. We also include the barrier heights calculated purely at the M06-2X/aug-cc-pVTZ level for comparison. The barriers calculated with M06-2X have a relatively good agreement to the CBS values with reverse barriers having better agreement. The agreements between M06-2X and CBS results are not as good as that was found for A1 in Table 2. For both A2 and A3 reactions, the M06-2X method overestimates the forward barrier by ~ 10 kJ/mol. That is $\sim 5.55\%$ and $\sim 6.37\%$ for A2 and A3, respectively. This directly affects the TST rate constants through the exponential parts of Eqs. 1 and 9 with or without the hindered rotor correction to the partition functions. The resulting M06-2X TST rate constants will be lower than the CBS TST ones over all temperatures. In the case of the 1D SCTST calculation, the larger barrier heights also reduce the tunneling probability, resulting in further underestimation of the rate constants comparing to the CBS results. The calculated rate constants for the A2 and A3 reactions are shown in Fig. 10(a) and (b) respectively. We can see the effect of quantum tunneling is more important at low T as expected. In addition, for both reactions, the calculation based on barrier heights without the CBS correction produces unreliable results.

Fig. 10(c) shows the 1D SCTST rate constants for the pericyclic H transfer reactions of all the group A simulant molecules. We can see that the pericyclic reaction for A2 is the fastest of the three, due to its smallest barrier height. The A1 and A3 reactions, having almost the same barrier heights (185.72 kJ/mol for A1 and 184.05 kJ/mol for A3), have almost the same

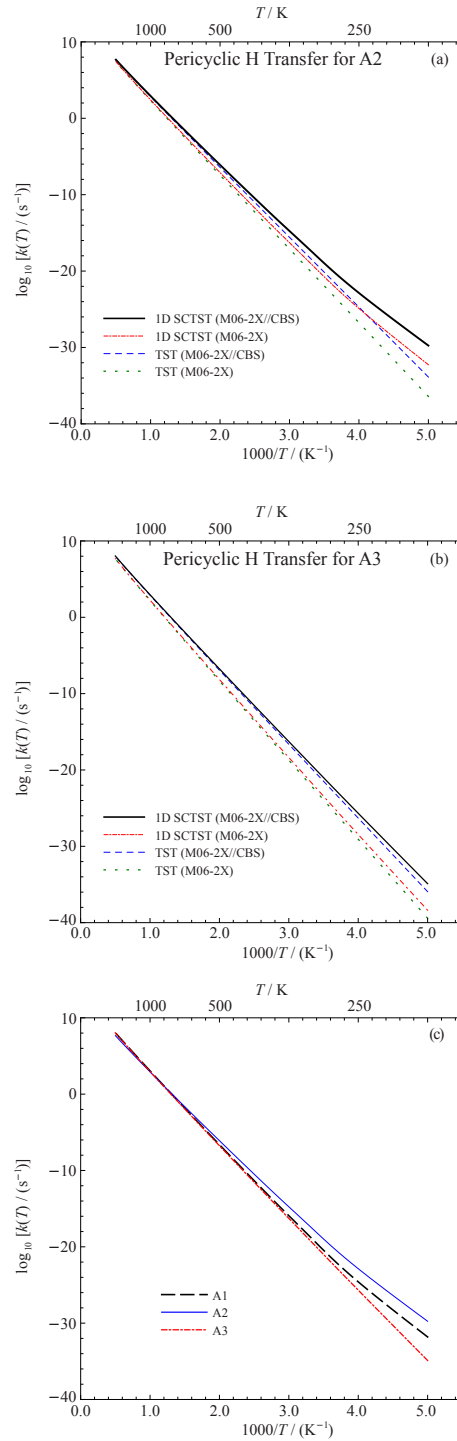


Figure 10: Reaction rate constants of the pericyclic H transfer in the temperature range from 200 K to 2000 K for (a) A2 and (b) A3, and (c) comparison of the 1D SCTST reaction rate constants for group A simulants.

rate constant at temperatures typically higher than 500 K. However, at lower temperature, it is clear that the A1 reaction is faster due to the SCTST tunneling correction. This is because of the difference between reaction mode vibrational frequencies, 1383.61(I) cm^{-1} for A1 and 934.01(I) cm^{-1} for A3, and smaller absolute value of this frequency in general leads to a wider approximated barrier and less tunneling. Comparing Figs. 6 and 10, one key conclusion can be drawn here is that although the M06-2X method significantly improves the B3LYP as seen in Figs. 5 and 6, it is important to perform the CBS single point energy calculation for the barrier heights, as the good agreement between M06-2X and CBS is not guaranteed.

4.3. Simulant B (*O,S*-Diethyl methylphosphonothiolate)

The conformer geometries of simulant B are reported in the Supporting Information. Although different conformer geometries of B are produced from rotation about four chemical bonds, C–O, O–P, S–P, and C–S, there are only 16 possible conformers due to steric hindrance between the groups at particular arrangement of the hindered rotation angles. This will also be found in the cases of the larger nerve agent molecules such as VX and VG, thus reducing the cost of calculations required for those molecules. We show in Fig. 11 the schematics of the reaction paths. Similar to VX, simulant B can carry out two steps of pericyclic H transfer reactions to reach the final product. Note that the P-containing product of the step 1 reactions is a chiral enantiomer of simulant A2 for the O-side and simulant A3 for the S-side. The chirality of the A group simulant molecule does not affect the kinetics or the thermodynamics. The second step reactions, being the same as A2 and A3, have been discussed already in Section 4.2. We therefore focus on only the first step reactions in this section.

The O-side and S-side TS’s conformer geometries can be found in the Supporting Information. There are 6 and 8 possible conformers for the O-side and S-side TS, respectively. The relative energies of the conformers are shown in Table 7. We note that majority of the

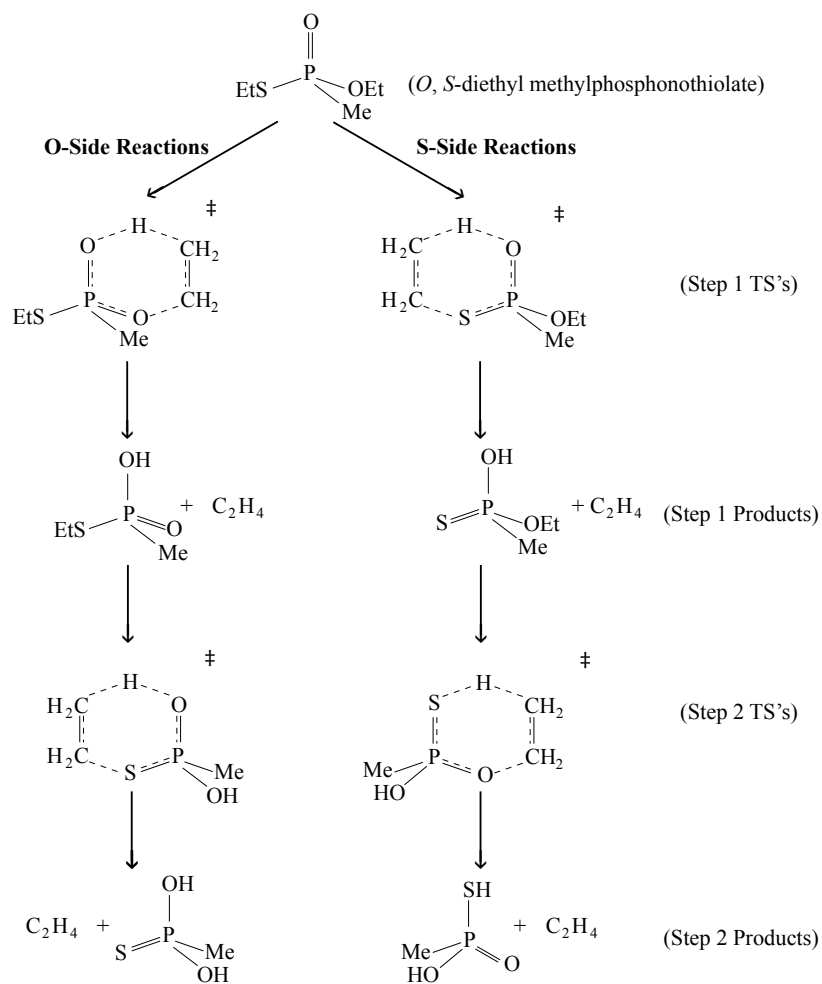


Figure 11: Schematics of proposed mechanisms of the pericyclic H-transfer reactions of simulant B. The abbreviations "Me", "Et", and "*i*-Pr" indicate the methyl, ethyl, and isopropyl groups, respectively.

conformers are relatively high in energy compared to the most stable one. The exception is the O-side TS’s with relative energies between all the conformers within 5 kJ/mol. In these conformers, the relative position of the ethyl group attached to the S atom is further away from the rest of the structure due to the relatively long bond lengths of the P–S and S–C bonds. Therefore, less steric hindrance effect is found in these conformers compared to the ones in the S-side TS conformers.

Table 7: Table of conformer relative energies of reactant and TS’s for the pericyclic H transfer reaction of simulant B. All values are in the unit of kJ/mol.

Reactant				O-side TS’s		S-side TS’s	
conf 1	0.00	conf 9	8.81	conf 1	0.00	conf 1	0.00
conf 2	0.402	conf 10	11.9	conf 2	3.93	conf 2	1.02
conf 3	5.76	conf 11	14.8	conf 3	2.41	conf 3	1.46
conf 4	11.1	conf 12	17.7	conf 4	2.10	conf 4	13.6
conf 5	11.1	conf 13	33.3	conf 5	2.48	conf 5	17.2
conf 6	15.7	conf 14	34.1	conf 6	0.386	conf 6	15.2
conf 7	12.4	conf 15	9.76			conf 7	19.2
conf 8	9.65	conf 16	21.9			conf 8	12.0

The reaction energetics are reported in Table 8. The S-side barrier height is lower than the O-side reaction by ~ 14 kJ/mol, while the S-side product is slightly higher in energy by ~ 7 kJ/mol. Note that comparing Fig. 11 and 3, simulants A1 and A2 can also be considered as the simulant molecules for the O-side and the S-side reactions respectively. The O-side forward barrier is ~ 4.6 kJ/mol ($\sim 2.4\%$) higher than that of simulant A1, while the S-side forward barrier being only ~ 1.3 kJ/mol ($\sim 0.75\%$) higher is even closer to that of the A2. It is also interesting to point out that the deviations of M06-2X/aug-cc-pVTZ barrier heights from that of the CBS/QB3 results are also similar to what we found for A1 and A2. In particular, the M06-2X/aug-cc-pVTZ barrier heights for the O-side reaction has excellent agreement to the CBS/QB3 results. For the S-side reaction, on the other hand, M06-2X/aug-cc-pVTZ underestimates the forward barrier by over 8 kJ/mol ($\sim 4.8\%$).

The calculated reaction rate constants for the O-side and S-side reactions are shown in Fig. 12(a) and (b) respectively. The two reactions have very similar reaction mode

Table 8: Table of reaction energetics of the pericyclic H transfer reaction for simulant B with geometries, vibrational frequencies, and energies calculated at M06-2X/aug-cc-pVTZ level. "CBS" indicates a single point energy correction at CBS/QB3 level is applied. All values are in the unit of kJ/mol.

	ΔV_f	ΔV_f (CBS)	ΔV_r	ΔV_r (CBS)
O-side	190.83	191.03	121.24	124.00
S-side	168.52	176.99	104.50	102.54

vibrational frequencies, 1396.66(I) cm^{-1} for the O-side and 1390.79(I) cm^{-1} for the S-side. These values are also very close to 1383.61(I) and 1388.05(I) cm^{-1} for A1 and A2 reactions respectively. These results show that A1 and A2 can be very good candidates of simulants for these two reactions. In order to further investigate this, we plot the A1 and A2 rate constants calculated at the same level of theory reported in previous sections in Fig. 12(a) and (b) respectively, and again show very good agreements between the rate constants of the A group simulants and the corresponding O/S-side reactions for simulant B. We also included the results at M06-2X/aug-cc-pVTZ level without high level single point energy corrections in these figures. We find excellent agreement of the 1D SCTST rate constants for the O-side reaction between the results with and without CBS correction. However, for the S-side reaction, the agreement is poor because of the underestimation of the reaction barrier without CBS correction shown in Table 8.

In Fig. 12(c) and its inset, we compare the calculated branching ratio of the two reactions using different methods. The TST and 1D SCTST branching ratio tend to converge for temperature higher than 300 K. Only at low T, we can see the difference of quantum tunneling contribution to the two reactions. For the O-side reaction shown in Fig. 12(c), the 1D SCTST branching ratio is higher than the TST one, indicating that the 1D SCTST estimates more quantum tunneling in this reaction than in the S-side reaction. Note that this comparison only indicates the relative contribution of quantum tunneling to the two reactions, not its absolute values. In the inset of Fig. 12(c), the 1D SCTST branching ratios of calculations with and without CBS corrections are compared. The calculation without

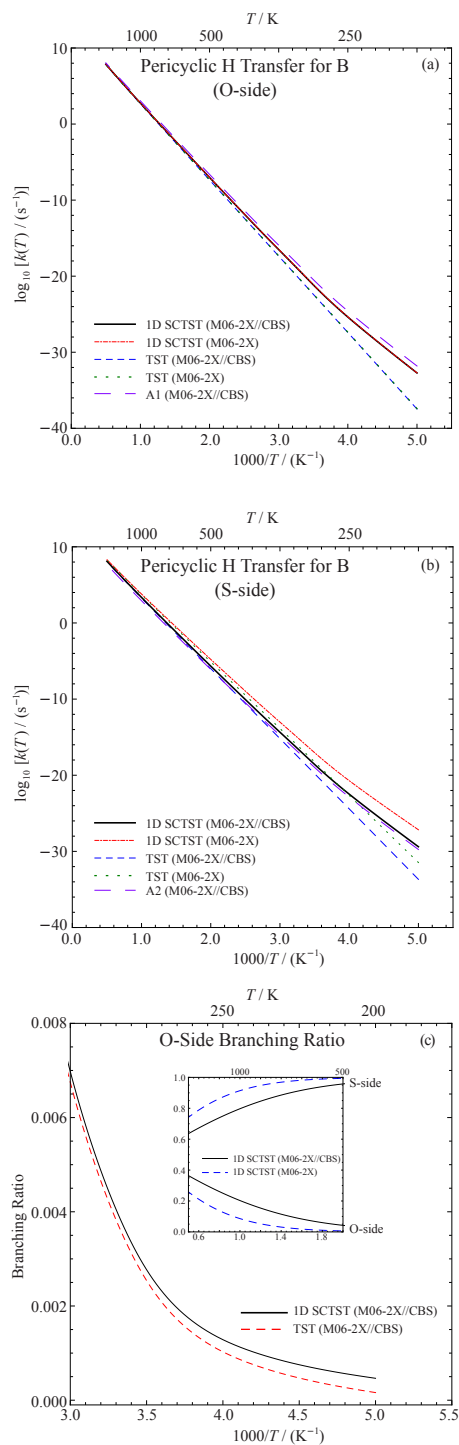


Figure 12: Reaction rate constants of the (a) O-side and (b) S-side pericyclic H transfer in the temperature range from 200 K to 2000 K for simulant B. (c) Comparison of calculated branching ratios between 1D SCTST and TST and in the inset between M06-2X/aug-cc-pVTZ and M06-2X/aug-cc-pVTZ//CBS/QB3.

CBS corrections consistently overestimates/underestimates the S-side/O-side branching ratios. This result once again shows that it is important to include the CBS single point energy corrections in the chemical kinetics calculation.

5. Conclusions

In this study, we investigated thermal decompositions of simulant molecules of the nerve agent VX. Since the ester and thioester side chains of VX is either an ethyl group or longer, it is very likely that VX will undergo two step pericyclic H transfer reactions at high temperatures. The loss of ethene from the *O*-ethyl group of VX upon electrospray ionisation in an ion trap mass spectrometer might occur through a similar mechanism.⁶⁵ We chose two groups of simulant molecules to study these reactions, in particular their macrocanonical rate constants. They were calculated using a combination of one-dimensional semiclassical transition state theory (1D SCTST) and multi-structure hindered rotor correction to the rovibrational partition function.

One of the simulant molecules, A1, was chosen as a test case for quantum chemistry calculations. We used results calculated at the MP2/jul-cc-pVTZ//CBS/QB3 level as the benchmark and tested DFT methods including B3LYP and M06-2X with 6-311++G(d,p), jul-cc-pVTZ, and aug-cc-pVTZ basis sets. We found that the M06-2X/aug-cc-pVTZ//CBS/QB3 results had the best agreement to the benchmark. In addition, for the test reaction, calculation at the M06-2X/aug-cc-pVTZ level without CBS correction to the energy showed very good agreement to the benchmark. However, according to our results for other simulant molecules, the energies computed at M06-2X/aug-cc-pVTZ level is not consistently accurate when comparing to the CBS results. For the first group simulants, the thioester (A2) had the smallest forward barrier and greatest rate constants over all temperatures. The simulant molecule in the second group, simulant B, had two possible pericyclic H transfer sites, an ester chain (O-side) and an thioester chain (S-side). Our calculation showed that the S-side

reaction was favoured both kinetically and thermodynamically. It dominated the reaction in the temperature range from 200 K to 2000 K.

We noted that two of the first group simulants, A1 and A2, were also simulants for the O-side and S-side reactions of simulant B, respectively. The calculated barrier heights for the two sites of simulant B were indeed very close to that of A1 and A2, respectively. We also compared the reaction rate constants for A1 and A2 reactions to the O-side and S-side B reactions and found very good agreement between them. This further showed that A1 and A2 are indeed reliable simulant molecules for studying kinetics of the first step pericyclic H transfer reactions for simulant B. We further speculate that the four simulant molecules studied in the current work are reliable for chemical kinetics investigations for the pericyclic H transfer reactions of VX.

Acknowledgement

X. Shan acknowledges the use of the University of Oxford Advanced Research Computing (ARC) facility in carrying out the theoretical studies in this work. X. Shan and D. C. Clary acknowledge support from DSTL Grant No. R1000121682. Content includes material subject to ©Crown copyright (2018), Dstl. This material is licensed under the terms of the Open Government Licence except where otherwise stated. To view this licence, visit <http://www.nationalarchives.gov.uk/doc/open-government-licence/version/3> or write to the Information Policy Team, The National Archives, Kew, London, TW9 4DU, or email psi@nationalarchives.gsi.gov.uk.

Supporting Information Available

The following files are available free of charge.

- Supporting Document: Optimized geometries of the stationary points of each reaction

at M06-2X/aug-cc-pVTZ level of theory

- Supporting Document: The data of reaction rate constants shown on Figs. 6, 10, and 12
- Supporting Document: The vibrational frequencies of the lowest energy conformer of the reactants and TS's for each reaction

This material is available free of charge via the Internet at <http://pubs.acs.org/>.

References

- (1) Kim, K.; Tsay, O. G.; Atwood, D. A.; Churchill, D. G. Destruction and Detection of Chemical Warfare Agents. *Chem. Rev.* **2011**, *111*, 5345–5403.
- (2) Timperley, C. M. *Best Synthetic Methods: Organophosphorus(V) Chemistry*; Elsevier: Oxford (UK), 2015.
- (3) Wilmsmeyer, A. R.; Gordon, W. O.; Davis, E. D.; Troya, D.; Mantooth, B. A.; Lalain, T. A.; Morris, J. R. Infrared Spectra and Binding Energies of Chemical Warfare Nerve Agent Simulants on the Surface of Amorphous Silica. *J. Phys. Chem. C* **2013**, *117*, 15685–15697.
- (4) Taylor, D. E.; Runge, K.; Cory, M. G.; Burns, D. S.; Vasey, J. L.; Hearn, J. D.; Griffith, K.; Henley, M. V. Surface Binding of Organophosphates on Silica: Comparing Experiment and Theory. *J. Phys. Chem. C* **2013**, *117*, 2699–2708.
- (5) Papas, B. N.; Petsalakis, I. D.; Theodorakopoulos, G.; Whitten, J. L. CI and DFT Studies of the Adsorption of the Nerve Agent Sarin on Surfaces. *J. Phys. Chem. C* **2014**, *118*, 23042–23048.
- (6) Le, N. Q.; Ekuma, C. E.; Dunlap, B. I.; Gunlycke, D. First-Principles Calculations of Sarin Adsorption on Anatase Surfaces. *J. Phys. Chem. C* **2018**, *122*, 2832–2839.

- (7) Kiddle, J. J.; Mezyk, S. P. Reductive Destruction of Chemical Warfare Agent Simulants in Water. *J. Phys. Chem. B* **2004**, *108*, 9568–9570.
- (8) Gershonov, E.; Columbus, I.; Zafrani, Y. Facile Hydrolysis-Based Chemical Destruction of the Warfare Agents VX, GB, and HD by Alumina-Supported Fluoride Reagents. *J. Org. Chem.* **2009**, *74*, 329–338.
- (9) Jang, Y. J.; Kim, K.; Tsay, O. G.; Atwood, D. A.; Churchill, D. G. Update 1 of: Destruction and Detection of Chemical Warfare Agents. *Chem. Rev.* **2015**, *115*, PR1–PR76.
- (10) Zboril, R.; Andrlé, M.; Oplustil, F.; Machala, L.; Tucek, J.; Filp, J.; Marusak, Z.; Sharma, V. K. Treatment of Chemical Warfare Agents by Zero-Valent Iron Nanoparticles and Ferrate(VI)/(III) Composite. *J. Hazard. Mater.* **2012**, *211-212*, 126–130.
- (11) Peterson, G. W.; Wagner, G. W. Detoxification of Chemical Warfare Agents by CuBTC. *J. Porous Mater.* **2014**, *21*, 121–126.
- (12) Bromberg, L.; Creasy, W. R.; McGarvey, D. J.; Wilusz, E.; Hatton, T. A. Nucleophilic Polymer and Gels in Hydrolytic Degradation of Chemical Warfare Agents. *ACS Appl. Mater. Interfaces* **2016**, *7*, 22001–22011.
- (13) Zhao, J.; Lee, D. T.; Yaga, R. W.; Hall, M. G.; Barton, H. F.; Woodward, I. R.; Oldham, C. J.; Walls, H. J.; W., P. G.; Parsons, G. N. Ultra-Fast Degradation of Chemical Warfare Agents Using MOF-Nanofiber Kebabs. *Angewandte Chemie - International Edition* **2016**, *55*, 13224–13228.
- (14) Gil-Sam-Millan, R.; López-Maya, E.; Hall, M.; Padial, N. M.; Peterson, G. W.; De-Coste, J. B.; Rodríguez-Albelo, L. M.; Oltra, J. E.; Barea, E.; Navarro, J. A. R. Chemical Warfare Agents Detoxification Properties of Zirconium Metal-Organic Frameworks by Synergistic Incorporation of Nucleophilic and Basic Sites. *ACS Appl. Mater. Interfaces* **2017**, *9*, 23967–23973.

- (15) Ash, T.; Debnath, T.; Banu, T.; Das, A. K. Exploration of Unimolecular Gas-Phase Detoxication Pathways of Sarin and Soman: A Computational Study from the Perspective of Reaction Energetics and Kinetics. *Chem. Res. Toxicol.* **2016**, *29*, 1439–1457.
- (16) Shan, X.; Vincent, J. C.; Kirkpatrick, S.; Walker, M. D.; Sambrook, M. R.; Clary, D. C. A Combined Theoretical and Experimental Study of Sarin (GB) Decomposition at High Temperatures. *J. Phys. Chem. A* **2017**, *121*, 6200–6210.
- (17) Bermudez, V. M. Quantum-Chemical Study of the Adsorption of DMMP and Sarin on γ -Al₂O₃. *J. Phys. Chem. C* **2007**, *111*, 3719–3728.
- (18) Kozlova, E. A.; Smirniotis, P. G.; Vorontsov, A. V. Comparative Study on Photocatalytic Oxidation of Four Organophosphorus Simulants of Chemical Warfare Agents in Aqueous Suspension of Titanium Dioxide. *J. Photochem. Photobiol. A* **2004**, *162*, 503–511.
- (19) Bermudez, V. M. Computational Study of Environmental Effects in the Adsorption of DMMP, Sarin, and VX on γ -Al₂O₃: Photolysis and Surface Hydroxylation. *J. Phys. Chem. C* **2009**, *113*, 1917–1930.
- (20) Yang, L.; Shroll, R. M.; Zhang, J.; Lourderaj, U.; Hase, W. L. Theoretical Investigation of Mechanisms for the Gas-Phase Unimolecular Decomposition of DMMP. *J. Phys. Chem. A* **2009**, *113*, 13762–13771.
- (21) Panayotov, D. A.; Morris, J. R. Thermal Decomposition of a Chemical Warfare Agent Simulant (DMMP) on TiO₂: Adsorbate Reactions with Lattice Oxygen as Studied by Infrared Spectroscopy. *J. Phys. Chem. C* **2009**, *113*, 15684–15691.
- (22) Mitchell, M. B.; Sheinker, V. N.; Cox, W. W., Jr.; Hardcastle, K. Sustained Room Temperature Decomposition of Dimethyl Methylphosphonate (DMMP) by O₃ on Alumina-Supported MnO_x. *J. Phys. Chem. C* **2011**, *115*, 11514–11524.

- (23) Yang, L.; Taylor, R.; de Jong, W. A.; Hase, W. L. A Model DMMP/TiO₂(110) Intermolecular Potential Energy Function Developed from *ab Initio* Calculation. *J. Phys. Chem. C* **2011**, *115*, 12403–12413.
- (24) Yang, L.; Tunega, D.; Xu, L.; Govind, N.; Sun, R.; Taylor, R.; Lischka, H.; de Jong, W. A.; Hase, W. L. Comparison of Cluster, Slab, and Analytical Potential Models for the Dimethyl Methylphosphonate (DMMP)/TiO₂(110) Intermolecular Interaction. *J. Phys. Chem. C* **2013**, *117*, 17613–17622.
- (25) Miller, W. H. Semiclassical Limit of Quantum Mechanical Transition State Theory for Nonseparable Systems. *J. Chem. Phys.* **1975**, *62*, 1899.
- (26) Miller, W. H. Semi-Classical Theory for Non-Separable Systems: Construction of “Good” Action-Angle Variables for Reaction Rate Constants. *Faraday Discuss. Chem. Soc.* **1977**, *62*, 40–46.
- (27) Miller, W. H. Recent Advances in Quantum Mechanical Reactive Scattering Theory, Including Comparison of Recent Experiments with Rigorous Calculations of State-to-State Cross Sections for the H/D+H₂ → H₂/HD + H Reactions. *Annu. Rev. Phys. Chem.* **1990**, *41*, 245–281.
- (28) Miller, W. H.; Hernandez, R.; Handy, N. C.; Jayatilaka, D.; Willetts, A. *Ab Initio* Calculation of Anharmonic Constants for a Transition State, with Application to Semi-classical Transition State Tunneling Probabilities. *Chem. Phys. Lett.* **1990**, *172*, 62–68.
- (29) Cohen, M. J.; Handy, N. C.; Hernandez, R.; Miller, W. H. Cumulative Reaction Probabilities for H + H₂ → H₂ + H from a Knowledge of the Anharmonic Force Field. *Chem. Phys. Lett.* **1992**, *192*, 407–416.
- (30) Nguyen, T. L.; Barker, J. R. Sums and Densities of Fully Coupled Anharmonic Vibrational States: A Comparison of Three Practical Methods. *J. Phys. Chem. A* **2010**, *114*, 3718–3730.

- (31) Nguyen, T. L.; Stanton, J. F.; Barker, J. R. *Ab Initio* Reaction Rate Constants Computed Using Semiclassical Transition-State Theory: $\text{HO} + \text{H}_2 \rightarrow \text{H}_2\text{O} + \text{H}$ and Isotopologues. *J. Phys. Chem. A* **2011**, *115*, 5118–5126.
- (32) Barker, J. R.; Nguyen, T. L.; Stanton, J. F. Kinetic Isotope Effects for $\text{Cl} + \text{CH}_4 \rightleftharpoons \text{HCl} + \text{CH}_3$ Calculated Using *Ab Initio* Semiclassical Transition State Theory. *J. Phys. Chem. A* **2012**, *116*, 6408–6419.
- (33) Weston, R. E., Jr.; Nguyen, T. L.; Stanton, J. F.; Barker, J. R. $\text{HO} + \text{CO}$ Reaction Rates and H/D Kinetic Isotope Effects: Master Equation Models with *ab Initio* SCTST Rate Constants. *J. Phys. Chem. A* **2013**, *117*, 821–835.
- (34) Greene, S. M.; Shan, X.; Clary, D. C. Reduced-Dimensionality Semiclassical Transition State Theory: Application to Hydrogen Atom Abstraction and Exchange Reactions of Hydrocarbons. *J. Phys. Chem. A* **2015**, *119*, 12015–12027.
- (35) Greene, S. M.; Shan, X.; Clary, D. C. An Investigation of One- Versus Two-Dimensional Semiclassical Transition State Theory for H Atom Abstraction and Exchange Reactions. *J. Chem. Phys.* **2016**, *144*, 084113.
- (36) Greene, S. M.; Shan, X.; Clary, D. C. Rate Constants of Chemical Reactions from Semiclassical Transition State Theory in Full and One Dimension. *J. Chem. Phys.* **2016**, *144*, 244116.
- (37) Shiekh, B. A.; Kaur, D. The Role of Torsional Motion on the Properties of Propiolic Acid and Its H/D Isotopic Analogs: A Density Functional Study Using SCTST and a Full Anharmonic VPT2 Model. *Chem. Phys. Lett.* **2016**, *646*, 168–173.
- (38) Shiekh, B. A.; Kaur, D.; Seth, B.; Mahajan, S. The Theoretical-Cum-Statistical Approach for the Investigation of Reaction $\text{NO}_2 + \text{O}(^3\text{P}) \leftarrow \text{NO} + \text{O}_2$ Using SCTST and a Full Anharmonic VPT2 Model. *Chem. Phys. Lett.* **2016**, *662*, 244–249.

- (39) Nguyen, T. L.; Stanton, J. F. High-level Theoretical Study of the Reaction Between Hydroxyl and Ammonia: Accurate Rate Constants from 200 to 2500 K. *J. Chem. Phys.* **2017**, *147*, 152704.
- (40) Shan, X.; Clary, D. C. Application of One-Dimensional Semiclassical Transition State Theory to the $\text{CH}_3 + \text{H} \rightleftharpoons \text{CH}_2\text{OH}/\text{CH}_3\text{O} + \text{H}_2$ Reactions. *Phil. Trans. R. Soc. A* **2017**, *376*, 20170147.
- (41) Drozd, G. T.; Kurtén, T.; Donahue, N. M.; Lester, M. I. Unimolecular Decay of the Dimethyl-Substituted Criegee Intermediate in Alkene Ozonolysis: Decay Time Scales and the Importance of Tunneling. *J. Phys. Chem. A* **2017**, *121*, 6036–6045.
- (42) Burd, T. A. H.; Shan, X.; Clary, D. C. Tunnelling and the Kinetic Isotope Effect in $\text{CH}_3 + \text{CH}_4 \rightarrow \text{CH}_4 + \text{CH}_3$: An Application of Semiclassical Transition State Theory. *Chem. Phys. Lett.* **2018**, *693*, 88–94.
- (43) Richardson, L. F.; Gaunt, J. A. The Deferred Approach to the Limit. Part I. Single Lattice. Part II. Interpenetrating Lattices. *Phil. Trans. R. Soc. Lond. A* **1927**, *226*, 299–361.
- (44) Ridders, C. Accurate Computation of $F'(x)$ and $F'(x)/F''(x)$. *Adv. Eng. Software* **1982**, *4*, 75–76.
- (45) Press, W. H.; Teukolsky, S. A.; Vetterling, W. T.; Flannery, B. P. *Numerical Recipes in C: The Art of Scientific Computing*, 2nd ed.; Cambridge University Press: Cambridge, 1992.
- (46) Miller, W. H. Tunneling Corrections to Unimolecular Rate Constants, with Application to Formaldehyde. *J. Am. Chem. Soc.* **1979**, *101*, 6810–6814.
- (47) Wagner, A. F. Improved Multidimensional Semiclassical Tunneling Theory. *J. Phys. Chem. A* **2013**, *117*, 13089–13100.

- (48) Ahmed, Z. Tunnelling through the Morse Barrier. *Phys. Lett. A* **1991**, *157*, 1–5.
- (49) Chuang, Y.-Y.; Truhlar, D. G. Statistical Thermodynamics of Bond Torsional Modes. *J. Chem. Phys.* **2000**, *112*, 1221–1228.
- (50) Ellingson, B. A.; Lynch, V. A.; Mielke, S. L.; Truhlar, D. G. Statistical Thermodynamics of Bond Torsional Modes: Tests of Separable, Almost-Separable, and Improved Pitzer-Gwinn Approximations. *J. Chem. Phys.* **2006**, *125*, 084305.
- (51) Zheng, J.; Truhlar, D. G. Kinetics of Hydrogen-Transfer Isomerizations of Butoxyl Radicals. *Phys. Chem. Chem. Phys.* **2010**, *12*, 7782–7793.
- (52) Zheng, J.; Yu, T.; Papajak, E.; Alecu, I. M.; Mielke, S. L.; Truhlar, D. G. Practical Methods for Including Torsional Anharmonicity in Thermochemical Calculations on Complex Molecules: The Internal-Coordinate Multi-Structural Approximation. *Phys. Chem. Chem. Phys.* **2011**, *13*, 10885–10907.
- (53) Pitzer, K. S.; Gwinn, W. D. Energy Levels and Thermodynamic Functions for Molecules with Internal Rotation I. Rigid Frame with Attached Tops. *J. Chem. Phys.* **1942**, *10*, 428–440.
- (54) Pitzer, K. S. Energy Levels and Thermodynamic Functions for Molecules with Internal Rotation II. Unsymmetrical Tops Attached to a Rigid Frame. *J. Chem. Phys.* **1946**, *14*, 239–243.
- (55) Kilpatrick, J. E.; Pitzer, K. S. Energy Levels and Thermodynamic Functions for Molecules with Internal Rotation III. Compound Rotation. *J. Chem. Phys.* **1949**, *17*, 1064–1075.
- (56) Gaussian 09 Revision E.01. Gaussian, Inc., Wallingford, 2009.
- (57) Papajak, E.; Zheng, J.; Xu, X.; Leverentz, H. R.; Truhlar, D. G. Perspectives on Basis

- Sets Beautiful: Seasonal Plantings of Diffuse Basis Functions. *J. Chem. Theory Comput.* **2011**, *7*.
- (58) Montgomery, J. A., Jr.; Frisch, M. J.; Ochterski, J. W.; Petersson, G. A. A Complete Basis Set Model Chemistry. VI. Use of Density Functional Geometries and Frequencies. *J. Chem. Phys.* **1999**, *110*, 2822–2827.
- (59) Montgomery, J. A., Jr.; Frisch, M. J.; Ochterski, J. W.; Petersson, G. A. A Complete Basis Set Model Chemistry. VII Use of the Minimum Population Localization Method. *J. Chem. Phys.* **2000**, *112*, 6532–6542.
- (60) Zhao, Y.; Truhlar, D. G. The M06 Suite of Density Functionals for Main Group Thermochemistry, Thermochemical Kinetics, Noncovalent Interactions, Excited States, and Transition Elements: Two New Functionals and Systematic Testing of Four M06-Class Functions and 12 Other Functionals. *Theor. Chem. Acc.* **2008**, *120*, 215–241.
- (61) Dunning, T. H., Jr. Gaussian Basis Sets for Use in Correlated Molecular Calculations. I. The Atoms Boron Through Neon and Hydrogen. *J. Chem. Phys.* **1989**, *90*, 1007–1023.
- (62) Dunning, T. H., Jr.; Peterson, K. A.; Wilson, A. K. Gaussian Basis Sets for Use in Correlated Molecular Calculations. X. The Atoms Aluminum Through Argon Revisited. *J. Chem. Phys.* **2001**, *114*, 9244–9253.
- (63) Clark, T.; Chandrasekhar, J.; Spitznagel, G. W.; Schleyer, P. V. R. Efficient Diffuse Function-Augmented Basis Sets for Anion Calculations. III. The 3-21+G Basis Set for First-Row Elements, Li-F. *J. Comp. Chem.* **1983**, *4*, 294–301.
- (64) Frisch, M. J.; Pople, J. A. Self-Consistent Molecular Orbital Methods 25. Supplementary Functions for Gaussian Basis Sets. *J. Chem. Phys.* **1984**, *80*, 3265–3269.
- (65) Bell, A. J.; Murrell, J.; Timperley, C. M.; Watts, P. Fragmentation and Reactions of Two Isomeric O-alkyl S-(2-dialkylamino)ethyl Methylphosphonothiolates Studied by Elec-

troscopy Ionization/Ion Trap Mass Spectrometry. *J. Am. Soc. Mass Spectrom* **2001**, *12*, 902–910.

Graphical TOC Entry

